1-1993

Study of D0 decays into K̄0 and K̄*0

M. PROCARIO

M. THULASIDAS
Singapore Management University, manojt@smu.edu.sg

Study of D^0 decays into $\bar{K}^0$ and $\bar{K}^{*0}$

M. Procario,[1] S. Yang,[1] D. S. Akerib,[2] B. Barish,[2] M. Chadha,[2] S. Chan,[2] D. F. Cowen,[2] G. Eigen,[2] J. S. Miller,[2] J. Urheim,[2] A. J. Weinstein,[2] D. Acosta,[3] M. Athanas,[3] G. Masek,[3] B. Ong,[3] H. Paar,[3] M. Sivertz,[3] A. Bean,[4] J. Gronberg,[4] R. Kutschke,[4] S. Menary,[4] R. J. Morrison,[4] S. Nakanishi,[4] H. N. Nelson,[4] T. K. Nelson,[4] J. D. Richman,[4] H. Tajima,[4] D. Schmidt,[4] D. Sperka,[4] M. S. Witherell,[4] R. Ballest,[5] M. Daoudi,[5] W. T. Ford,[5] D. R. Johnson,[5] K. Lingel,[5] M. Lohner,[5] P. Rankin,[5] J. G. Smith,[5] J. P. Alexander,[6] C. Bebek,[6] K. Berkelman,[6] D. Besson,[6] T. E. Browder,[6] D. G. Cassel,[6] H. A. Cho,[6] D. M. Coffman,[6] P. S. Drell,[6] R. Ehrlich,[6] R. S. Galik,[6] M. Garcia-Sciveres,[6] B. Geiser,[6] B. Gittelman,[6] S. W. Gray,[6] D. L. Hartill,[6] B. K. Heltsley,[6] K. Honscheid,[6] C. D. Jones,[6] S. L. Jones,[6] J. Kandaswamy,[6] N. Katayama,[6] P. C. Kim,[6] D. L. Kreinick,[6] G. S. Ludwig,[6] J. Masui,[6] J. Mevissen,[6] N. B. Mistry,[6] C. R. Ng,[6] E. Nordberg,[6] M. Ogg,[6,*] C. O'Grady,[6] J. R. Patterson,[6] D. Peterson,[6] D. Riley,[6] M. Sapper,[6] M. Selen,[6] H. Worden,[6] M. Worris,[6] F. Würthwein,[6] P. Avery,[7] A. Freyberger,[7] J. Rodriquez,[7] R. Stephens,[1] J. Yelton,[7] D. Cinabro,[8] S. Henderson,[8] K. Kinoshita,[8] T. Liu,[8] M. Saulnier,[8] R. Wilson,[8] H. Yamamoto,[8] A. J. Sadoff,[9] R. Ammar,[10] S. Ball,[10] P. Baringer,[10] D. Coppage,[10] N. Copty,[10] R. Davis,[10] N. Hancock,[10] M. Kelly,[10] N. Kwak,[10] H. Lam,[10] Y. Kubota,[11] M. Lattery,[11] J. K. Nelson,[11] S. Patton,[11] D. Perticone,[11] R. Poling,[11] V. Savinov,[11] S. Schrenk,[11] R. Wang,[11] M. S. Alam,[12] I. J. Kim,[12] B. Nemati,[12] J. J. O'Neill,[12] V. Romero,[12] H. Severini,[12] C. R. Sun,[12] M. M. Zoeller,[12] G. Crawford,[13] R. Fulton,[13] K. K. Gan,[13] H. Kagan,[13] R. Kass,[13] J. Lee,[13] R. Malchow,[13] F. Morrow,[13] Y. Skovpen,[13,†] M. Sung,[13] C. White,[13] J. Whitmore,[13] P. Wilson,[13] F. Butler,[14] X. Fu,[14] G. Kalbfleisch,[14] M. Lambrecht,[14] W. R. Ross,[14] P. Skubic,[14] J. Snow,[14] P. L. Wang,[14] M. Wood,[14] D. Bortoletto,[15] D. N. Brown,[15] J. Dominick,[15] R. L. McIlwain,[15] T. Miao,[15] D. H. Miller,[15] M. Modesitt,[15] S. F. Schaffner,[15] E. I. Shibata,[15] I. P. J. Shipsey,[15] P. N. Wang,[15] M. Battle,[16] J. Ernst,[16] H. Kroha,[16] S. Roberts,[16] K. Sparks,[16] E. H. Thorndike,[16] C. H. Wang,[16] S. Sanghera,[17] T. Skwarnicki,[17] R. Stroynowski,[17] M. Artuso,[18] M. Goldberg,[18] N. Horwitz,[18] R. Kennett,[18] G. C. Moneti,[18] F. Muheim,[18] S. Playfer,[18] Y. Rozen,[18] P. Rubin,[18] S. Stone,[18] M. Thulasidas,[18] G. Zhu,[18] A. V. Barnes,[19] J. Bartelt,[19] S. E. Csorna,[19] Z. Egyed,[19] V. Jain,[19] and P. Sheldon[19]

(CLEO Collaboration)

[1]*Carnegie-Mellon University, Pittsburgh, Pennsylvania 15213*
[2]*California Institute of Technology, Pasadena, California 91125*
[3]*University of California, La Jolla, California 92093*
[4]*University of California, Santa Barbara, California 93106*
[5]*University of Colorado, Boulder, Colorado 80309-0390*
[6]*Cornell University, Ithaca, New York 14853*
[7]*University of Florida, Gainesville, Florida 32611*
[8]*Harvard University, Cambridge, Massachusetts 02138*
[9]*Ithaca College, Ithaca, New York 14850*
[10]*University of Kansas, Lawrence, Kansas 66045*
[11]*University of Minnesota, Minneapolis, Minnesota 55455*
[12]*State University of New York at Albany, Albany, New York 12222*
[13]*Ohio State University, Columbus, Ohio 43210*
[14]*University of Oklahoma, Norman, Oklahoma 73019*
[15]*Purdue University, West Lafayette, Indiana 47907*
[16]*University of Rochester, Rochester, New York 14627*
[17]*Southern Methodist University, Dallas, Texas 75275*
[18]*Syracuse University, Syracuse, New York 13244*
[19]*Vanderbilt University, Nashville, Tennessee 37235*

(Received 14 October 1992)

Using the CLEO II detector at CESR we have studied D^0 decays into final states with a $\bar{K}^0$ or $\bar{K}^{*0}$, and have measured branching ratios for the decay modes $D^0 \to (\bar{K}^0/\bar{K}^{*0})\pi^0, \eta, \eta'$. These results are compared with predictions of various charm decay models, and contributions of final-state interactions are discussed.

PACS number(s): 13.25.+m, 14.40.Jz

*Permanent address: Carleton University, Ottawa, Canada. †Permanent address: INP, Novosibirsk, Russia.

I. INTRODUCTION

Nonleptonic decays of charm mesons have challenged theoretical explanation for some time; in particular, the lifetime difference between D^0 and D^+ was not explainable. Recently, several models [1–6] have emerged which have enjoyed moderate success in explaining these decays. Some of these models [1,4] use the factorization approach, where the meson decay amplitude is constructed out of two independent hadronic currents. This approach works well in describing decays which have "external" W spectator diagrams, as in Fig. 1(a), but not for "internal" W spectator diagrams [Fig. 1(b)]. The other models, $1/N$ ansatz [5] and QCD sum rules [2], have a stronger theoretical basis than the factorization approach and also give a good general description of charm decays but still suffer from deficiencies. For instance, none of the models can reliably predict the contributions of "W-exchange" diagrams [Fig. 1(c)] or account for the effects of final-state interactions (FSI's). There are indications that FSI's play an important role in charm meson decays, as evidenced by the measured [7] branching ratio for $D^0 \to \bar{K}^0 \phi$ ($\approx 1\%$), which is too large to be explained by the lowest-order (W-exchange) diagrams.

The decay mode $D^0 - \bar{K}^{*0}\eta$ is particularly well suited for studying the effects of final-state interactions. When $D^0 \to \bar{K}^0 \phi$ was detected [7], it was thought to be evidence for a W-exchange process, as shown in Fig. 2(a). However, Donoghue [8] argued that this final state could occur via final-state interactions as in Fig. 2(b). He pointed out that, given $\mathcal{B}(D^0 \to \bar{K}^0 \phi) \approx 1\%$, the intermediate state $D^0 \to \bar{K}^{*0}\eta$ should have a branching ratio of at least 2%. The factorization approach [1] predicted 0.3% for the $\bar{K}^{*0}\eta$ final state, but using the measured branching ratio for $D^0 \to \bar{K}^0 \phi$ as input (and as a quantitative measure of final-state interactions) the authors increased the prediction to 2.5%. One can also have significant contributions from final-state interactions in $D^0 \to PP$ decays (P is a pseudoscalar), e.g., $\mathcal{B}(D^0 - \bar{K}^0 \pi^0)/B(D^0 \to K^- \pi^+)$ was expected [9] to be $\frac{1}{40} - \frac{1}{18}$ from naive color counting, whereas experimentally [7] this ratio is closer to 0.6. Further, Lipkin [10,11] has suggested that the ratio $\mathcal{B}(D \to M\eta)/B(D \to M\eta')$ can be used to test the contribution of W-annihilation diagrams and final-state interactions, where D is any charmed meson and M is any noncharmed meson.

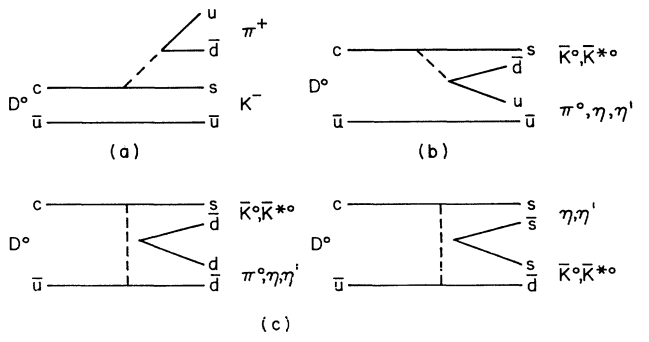

FIG. 1. Feynman diagrams for (a) external W process, (b) internal W process, (c) W-exchange process.

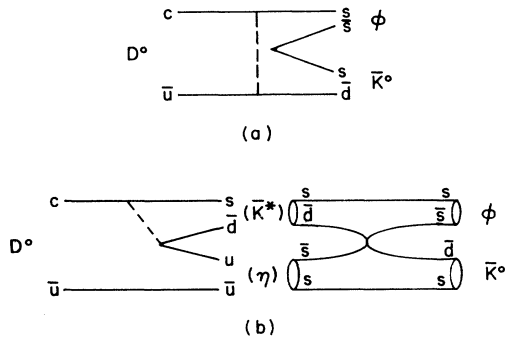

FIG. 2. Feynman diagram for $D^0 \to \bar{K}^0 \phi$ (a) via W exchange, (b) via final-state interactions.

In this paper, we report new measurements for D^0 decays for PP or PV final states containing a $\bar{K}^0$ or $\bar{K}^{*0}$ and nonstrange neutrals π^0, η, or η' in the final state (mention of any reaction also implies its charge conjugate partner). In lowest order, all these decay modes occur either through "internal W-emission-" or "W-exchange-" type diagrams, as shown in Figs. 1(b)–1(c).

II. DATA SAMPLE AND EVENT SELECTION

The data used in this analysis were collected by the CLEO II detector operating at the Cornell Electron Storage Ring (CESR), and correspond to an integrated luminosity of 1540 pb^{-1}. The data were taken at center-of-mass energies between 10.36 and 10.70 GeV, which correspond to the $\Upsilon(3S)$ and the continuum above the $\Upsilon(4S)$ resonances.

The CLEO II detector detects neutral and charged particles with excellent resolution and efficiency. The detector consists of a tracking system surrounded by time of flight scintillation counters and an electromagnetic calorimeter, which are immersed in a 1.5 T solenoidal magnetic field generated by a superconducting coil. The magnet coil is surrounded by iron slabs and muon counters. A detailed description of the detector can be found elsewhere [12].

Events are selected using the standard CLEO hadronic selection criteria [13]. Pion and kaon candidates are required to have ionization losses within 2.5 standard deviations of the expected values. $\bar{K}^0$'s are detected as K_S^0's in the $K_S^0 \to \pi^+\pi^-$ final state. K_S^0 candidates are selected by choosing two tracks of opposite charge which intersect at least 1 mm away from the interaction point in a plane transverse to the beam. The invariant mass of these tracks, assumed to be pions, is required to be within 3σ ($\sigma \approx 3.7$ MeV/c^2) of the known K_S^0 mass.

Photons are detected by the electromagnetic calorimeter which consists of 7800 thallium-doped CsI crystals. To select $\pi^0 \to \gamma\gamma$ decays, we choose only those photons which have energies greater than 30 MeV and cannot be matched to a charged track. Since photon rates are higher and the energy resolution is poorer in the end cap

region of the calorimeter relative to the barrel region, one photon is restricted to be in the barrel (71% of the solid angle), whereas the other photon is allowed to be in either the barrel or the good resolution part of the end cap (91% of the solid angle). We keep all $\gamma\gamma$ combinations, whose invariant mass is within 2σ of the π^0 mass, where σ is typically 5–6 MeV/c^2. In order to improve the momentum resolution of the π^0, the selected $\gamma\gamma$ pairs are kinematically constrained to the nominal π^0 mass.

For $D^0\to\bar{K}^0/\bar{K}^{*0}\eta$ final states, where $\eta\to\gamma\gamma$, the η candidates are selected in a manner similar to the π^0's, but with the additional constraint that photons which could be paired to make π^0's with momentum greater than 0.8 GeV/c are rejected. We also detect η's using the $\eta\to\pi^+\pi^-\pi^0$ decay chain. For this mode, P_{π^0} is required to be greater than 0.3 GeV/c. All η candidates within 2σ of the nominal mass are considered, where typical values of σ are around 14 MeV/c^2 for the $\gamma\gamma$ mode, and 6 MeV/c^2 for the $\pi^+\pi^-\pi^0$ mode. In order to improve the η momentum resolution, the selected $\gamma\gamma$ pairs are kinematically constrained to the nominal η mass.

To select η' candidates we use the $\rho\gamma$ and $\eta\pi\pi$ final states. The combinatoric background under the η' peak is reduced by using somewhat tighter cuts for the γ, π^0, and η's. The ρ candidate mass [14] is required to lie between 500 and 850 MeV/c^2, and the photon energy must exceed 0.1 GeV. If a candidate γ forms a π^0 with any other γ (with $E_\gamma>0.2$ GeV), then it is rejected. Since the η' is spinless and the photon is transversely polarized, the ρ is also transversely polarized. We thus restrict the ρ helicity angle, θ, such that $|\cos\theta|<0.8$ [θ is the angle between one of the π's (from the ρ) and the η' in the ρ rest frame]. We require the η' momentum to be above 0.5 GeV/c, and its mass to be within 3σ of the nominal mass, where σ is typically 10 MeV/c^2. In order to improve the η' momentum resolution, the selected $\pi^+\pi^-\gamma$ combinations are constrained to the η' mass. We also select η's using the $\eta\pi^+\pi^-$ mode, where the η is detected in both $\gamma\gamma$ and $\pi^+\pi^-\pi^0$ modes. The η candidates are chosen if they are within 3σ of the nominal mass. For the $\eta\to\gamma\gamma$ mode, the energy of both photons must exceed 0.1 GeV, and if either can be paired with another photon to make a π^0 with $P_{\pi^0}>0.4$ GeV/c, it is rejected. The $\gamma\gamma$ pairs are kinematically fitted to the nominal η mass to improve the latter's momentum resolution.

Candidate $\bar{K}^{*0}$'s are selected using both $\bar{K}^0\pi^0$ and $K^-\pi^+$ decay modes. In fitting the $K\pi$ mass plots, we fix the mass of the $\bar{K}^{*0}$ to 896 MeV/c^2 (Particle Data Group value [7]). To determine the width of the $\bar{K}^{*0}$ we used the entire data sample, where we fitted all $\bar{K}^0\pi^0$ and $K^-\pi^+$ mass combinations in various momentum bins, and thus obtained an average width of 57 and 55 MeV/c^2 for the two modes, respectively.

III. DECAYS CONTAINING $\bar{K}^0$

A. $D^0\to\bar{K}^0\pi^0$

The invariant mass distribution of $K_S^0\pi^0$ combinations is shown in Fig. 3 for $X_{D^0}\geq 0.5$, where $X_{D^0}=P_{D^0}/E_{\text{beam}}$.

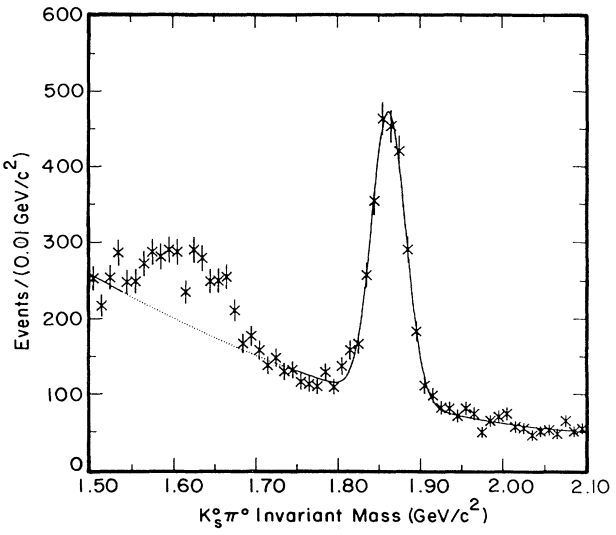

FIG. 3. Invariant mass of $K_S^0\pi^0$ combinations, for $X_{D^0}\geq 0.5$.

Charm production in the continuum peaks at high momentum, thus the X cut reduces the combinatoric background. Since the D^0 is spinless, the cosine of the angle (θ) of the K_S^0 (or π^0) in the D^0 rest frame with respect to the D^0 laboratory momentum is uniformly distributed, whereas in the data the background peaks at $\cos\theta\approx 1.0$. We require $\cos\theta<0.8$. The excess of events in the region 1.5–1.7 GeV/c^2 is due to feed-down from reactions like $D^0\to\bar{K}^0\pi^0\pi^0$, $D^+\to\bar{K}^0\rho^+$ ($\rho\to\pi^+\pi^0$) where one of the pions is not used. We exclude this region from the fit and use a gaussian for the signal and a polynomial for the background shape. Table I presents information on the detected signal and efficiency [15] of this mode. The efficiency includes the branching ratio of $\bar{K}^0$ into the observed decay mode ($\pi^+\pi^-$).

To obtain a branching ratio for this mode, we normalize it to $D^0\to\bar{K}^0\pi^+\pi^-$ (branching ratio [16] = 6.4±1.1%), and obtain

$$\frac{\mathcal{B}(D^0\to\bar{K}^0\pi^0)}{\mathcal{B}(D^0\to\bar{K}^0\pi^+\pi^-)}=0.44\pm0.02\pm0.05\ .$$

This implies $\mathcal{B}(D^0\to\bar{K}^0\pi^0)=2.8\pm0.1\pm0.6\%$. Normalizing to the $\bar{K}^0\pi^+\pi^-$ final state eliminates most of the systematic effects associated with vee finding. A portion of the systematic error is estimated by varying the selection criteria, e.g., by imposing different momentum cuts on the D^0 candidate, and by requiring different cuts on $\cos\theta$. We also did the analysis by requiring the D^0 to come from a D^{*+}. In all cases, we obtained results which agreed with the value quoted here. The systematic error also includes the error in the branching ratio of the normalizing mode. See the Appendix for a numerical breakdown of the systematic error. In Table II, we present this measurement and compare it to previous measurements and theoretical estimates. The Bauer-

TABLE I. Signal and efficiency for final states with $\bar{K}^0$.

D decay mode	Decay mode of D^0 daughters	Number of events in signal	$\epsilon\mathcal{B}$[a]
$\bar{K}^0\pi^0$		1942±64	6.8±0.2%
$\bar{K}^0\eta$	$\eta\to\gamma\gamma$	225±30	2.5±0.1%
	$\eta\to\pi^+\pi^-\pi^0$	80±12	0.91±0.07%
$\bar{K}^0\eta'$	$\eta'\to\rho\gamma$	372±45	1.63±0.06%
$\bar{K}^0\eta'$	$\eta'\to\eta\pi^+\pi^-$		
	$\eta\to\gamma\gamma$	168±15	0.85±0.03%
$\bar{K}^0\eta'$	$\eta'\to\eta\pi^+\pi^-$		
	$\eta\to\pi^+\pi^-\pi^0$	54±9	0.32±0.02%
$\bar{K}^0\pi^+\pi^-$		6500±171	10.1±0.3%

[a]$\epsilon\mathcal{B}$ is the product of the efficiency to reconstruct this made and the branching ratio of the D^0 daughter to observable particles.

Stech-Wirbel (BSW) model [1] uses a branching ratio of 2.5% for this mode as an input. This value is based on previous measurements. Our result agrees with this choice.

B. $D^0\to\bar{K}^0\eta$

Using the $\gamma\gamma$ mode for η, we construct $K_S^0\eta$ mass combinations as shown in Fig. 4(a), for $X_{D^0}\geq 0.5$. In addition, we require that the cosine of the angle of the K_S^0 in the D^0 rest frame with respect to the D^0 laboratory momentum be less than 0.7. Fitting with a gaussian and a polynomial for the signal and background, respectively, we obtain 225±30 events. Table I contains more information on this decay mode. Normalizing the signal to our measurement of $D^0\to\bar{K}^0\pi^0$ eliminates most of the systematics associated with tagging K_S^0's and kinematic fitting of $\gamma\gamma$ combinations. We obtain

$$\frac{\mathcal{B}(D^0\to\bar{K}^0\eta)}{\mathcal{B}(D^0\to\bar{K}^0\pi^0)}=0.32\pm0.04\pm0.03 .$$

We also reconstruct the η in the $\pi^+\pi^-\pi^0$ final state, as shown in Fig. 4(b). Requiring the same cuts on the D^0 momentum and the K_S^0 angle, we obtain 80±12 events. (See Table I for details on this decay mode.) Normalizing to $D^0\to\bar{K}^0\pi^+\pi^-$, we obtain

$$\frac{\mathcal{B}(D^0\to\bar{K}^0\eta)}{\mathcal{B}(D^0\to\bar{K}^0\pi^+\pi^-)}=0.14\pm0.02\pm0.02 .$$

Using our measurement for $\mathcal{B}(D^0\to\bar{K}^0\pi^0)$ and the Mark III result [16] for $\mathcal{B}(D^0\to\bar{K}^0\pi^+\pi^-)$, and averaging the two results [17], we find $\mathcal{B}(D^0\to\bar{K}^0\eta)=0.88\pm0.09\pm0.19\%$. The systematic error includes the effects of varying the selection criteria, errors in the normalizing mode, and uncertainties in the Monte Carlo simulation [18]. See the Appendix for a numerical breakdown of the systematic error. A comparison of this result with other results is presented in Table II.

C. $D^0\to\bar{K}^0\eta'$

This mode is reconstructed most cleanly when the η' is detected in the $\eta\pi^+\pi^-$ mode, where $\eta\to\gamma\gamma$. The η's were also reconstructed in the $\pi^+\pi^-\pi^0$ mode. We also used the $\rho\gamma$ final state to tag η' candidates. In Fig. 5, we show the $K_S^0\eta'$ invariant mass distribution for $X_{D^0}>0.5$ for the three submodes. In Table I, we present the number of detected events and the efficiency of each of these three submodes.

To obtain a branching ratio for $D^0\to\bar{K}^0\eta'$, we average

TABLE II. Comparison of results for final states with $\bar{K}^0$.

Results	$\bar{K}^0\pi^0$	$\bar{K}^0\eta$	$\bar{K}^0\eta'$
This result	2.8±0.1±0.6%	0.88±0.09±0.19%	2.0±0.15±0.42%
Previous results			
ARGUS [20]		<2.7%(90% C.L.)	
CLEO [21]	2.3±0.3±0.6%		
E691 [22]	5.7±1.0±1.2%		
ARGUS [23]	2.2±0.3±0.5%		2.4±0.8±0.6%
Theory			
WSB without FSI's [1]	1%	0.4%	0.15%
WSB with FSI's [1]	input 2.5%		
$1/N$, $N=\infty$ [5,24]	2.1%	0.8%	
$1/N$, $N=3$	0.2%	0.1%	
QCD sum rules [2]	1.5%	0.4%	1.2%

[19] the results from the three submodes. Normalizing this mode to $D^0 \to \bar{K}^0 \pi^+ \pi^-$, we obtain

$$\frac{\mathcal{B}(D^0 \to \bar{K}^0 \eta')}{\mathcal{B}(D^0 \to \bar{K}^0 \pi^+ \pi^-)} = 0.31 \pm 0.02 \pm 0.04 \ .$$

This corresponds to $\mathcal{B}(D^0 \to \bar{K}^0 \eta') = 2.0 \pm 0.15 \pm 0.42\%$. The systematic error arises from several sources: uncertainty in track-finding efficiency as a function of momentum and angle, uncertainty in photon-finding efficiency as a function of momentum, and uncertainty in the matrix elements used in the η' modeling (e.g., the ρ line shape in $\eta' \to \rho\gamma$, and the dipion mass spectrum in $\eta' \to \eta^0 \pi^+ \pi^-$), and uncertainty in the net branching ratio of the η' mode used. Conveniently, the three η' submodes that we measure span a wide range in both photon and charged track momentum. We therefore use the dispersion in the branching ratios we obtain from the three submodes as a measure of the systematic error in our overall measurement of $D^0 \to \bar{K}^0 \eta'$, cognizant that this is a measure of the momentum and angle acceptance of our detector. The systematic error also includes the error in the branching ratio of the normalizing mode. In Table II, we compare this result with other experimental results and theoretical predictions.

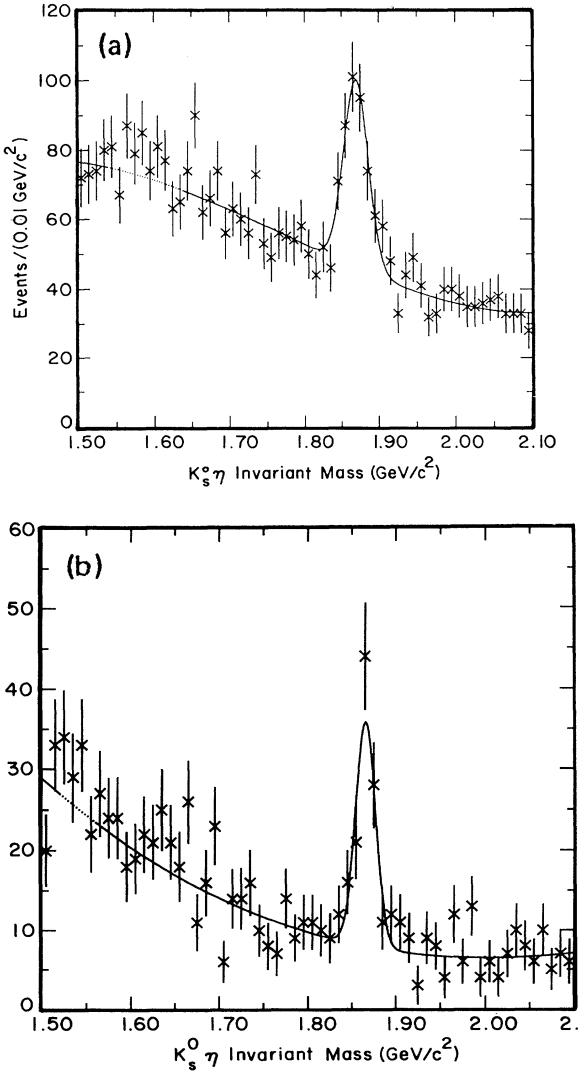

FIG. 4. Invariant mass of $K_S^0 \eta$ combinations: (a) $\eta \to \gamma\gamma$, (b) $\eta \to \pi^+ \pi^- \pi^0$ for $X_{D^0} \geq 0.5$.

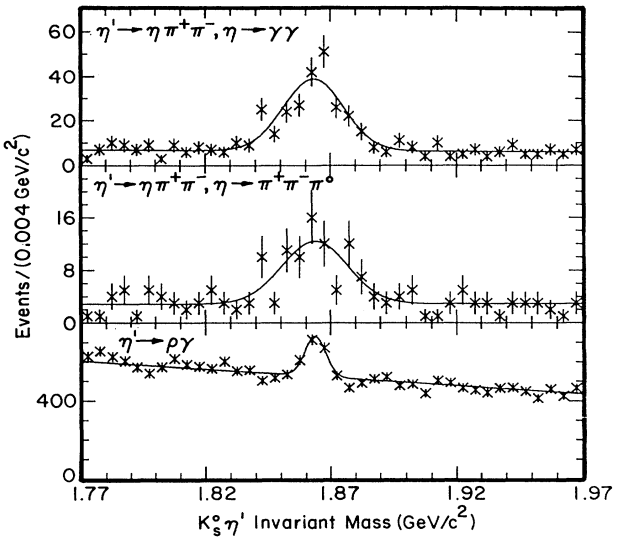

FIG. 5. Invariant mass of $K_S^0 \eta'$ combinations, for $X_{D^0} \geq 0.5$ for the three submodes.

IV. DECAYS CONTAINING $\bar{K}^{*0}$

A. $D^0 \to \bar{K}^{*0} \pi^0$

This mode has been previously studied by the Mark III Collaboration [25]; its branching ratio was extracted via a Dalitz plot analysis of the reaction $D^0 \to K^- \pi^+ \pi^0$, where the amplitude for $\bar{K}^{*0} \pi^0$ interferes with $K^{*-} \pi^+$, $K^- \rho^+$ and nonresonant $K^- \pi^+ \pi^0$ [$(K^- \pi^+ \pi^-)_{\rm NR}$]. In contrast, we use the reaction $D^0 \to \bar{K}^0 \pi^0 \pi^0$, where the interference is between $\bar{K}^{*0}(892)\pi^0$, $(\bar{K}^0 \pi^0 \pi^0)_{\rm NR}$, and possibly [26] $\bar{K}_0^*(1430)\pi^0$. The Mark III result [25] for $D^+ \to K^- \pi^+ \pi^+$ was reanalyzed [27], and it was pointed out that the experimental mass distributions would be better explained if the amplitude for $\bar{K}_0^*(1430)\pi^0$ was included in the Dalitz plot fit. Since the decay of $\bar{K}_0^*(1430)$ to $K^- \pi^+$ and $\bar{K}^0 \pi^0$ is related by isospin, we search for it in the $K_S^0 \pi^0 \pi^0$ final state.

We determine the fractions of resonant and nonresonant three-body contributions to the decay mode by fitting the Dalitz plot distributions to a coherent sum of amplitudes, using the maximum likelihood method. Since there are two identical pions in the final state, the amplitudes for the resonant decays must be symmetrized with respect to the exchange of the two pions. The Dalitz plot fit is done separately to the D signal region (1.82–1.90 GeV/c^2) and to the D sideband regions

(1.75–1.79 and 1.93–1.97 GeV/c^2); the signal region contains 206 events, whereas the sideband regions contain 69 events. The fit to the D sideband region is done to parametrize the background under the D peak.

In order to reduce background, the D^0 is required to come from a D^{*+}. We require $X_{D^{*+}} > 0.5$, and the mass difference $M_{D^{*+}} - M_{D^0}$ is restricted to be within ± 2.0 MeV/c^2 of the nominal value ($\sigma \approx 0.7$ MeV/c^2). In addition, the two pions must have energies greater than 0.35 GeV. In Fig. 6 we show the $\bar{K}^0\pi^0\pi^0$ invariant mass, and in Fig. 7 the Dalitz plot for events in the D signal region, which includes both the D peak and the background under the D peak. Since there are two identical pions in the final state, the two $K_S^0\pi^0$ combinations are plotted per event, one as the low mass and one as the high mass combination.

The likelihood functions for events in the D peak and background under the D peak, can be written as

$$\mathcal{L}_s = |\sqrt{(f_1)}e^{i\phi_1}A_{3b} + \sqrt{(f_2)}e^{i\phi_2}(\mathrm{BW}_{\bar{K}^{*0}(892)})|^2 ,$$

$$\mathcal{L}_b = [g_1 B_{3b}^2 + g_2(\mathrm{BW}_{\bar{K}^{*0}(892)})^2] ,$$

where f_i, g_i are the various fit fractions [28], ϕ_i are the phase angles, A_{3b} is the three-body nonresonant contribution to events in the D peak, B_{3b} describes the combinatoric background under the D peak, and the BW's are the Breit-Wigner functions for the resonant contribution.

Both A_{3b} and B_{3b} are constants across the phase space and hence are set to unity. We also set $f_1 = g_1 = 1$ and $\phi_1 = 0$. We thus measure the fraction and phase of the resonance relative to the non-resonant part. The value of the parameters in $\mathcal{L}_b$ are obtained by fitting to the D sideband region, where we do not allow for any interference among the amplitudes. In fitting the signal region, we use the function

$$\mathcal{L} = \frac{R\mathcal{L}_s + \mathcal{L}_b}{R+1} ,$$

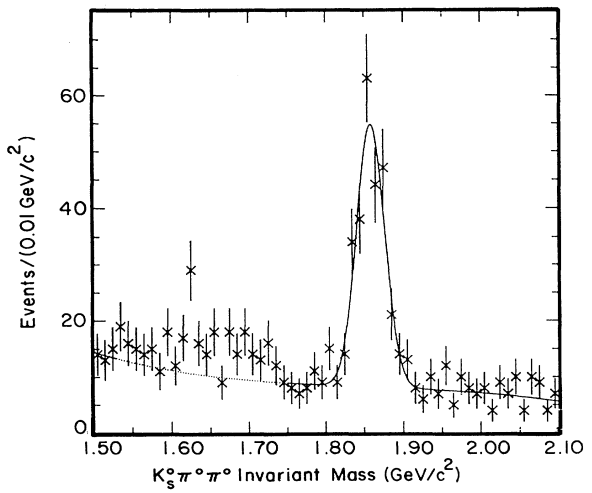

FIG. 6. $\bar{K}^0\pi^0\pi^0$ invariant mass for $X_{D^{*+}} \geq 0.5$.

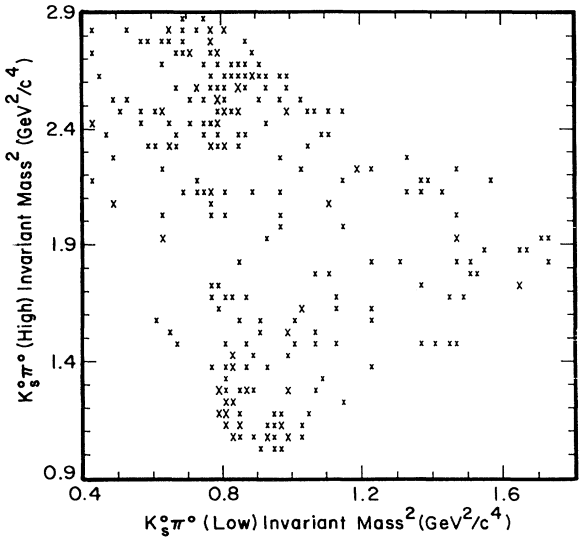

FIG. 7. Dalitz plot for $\bar{K}^0\pi^0\pi^0$, where events are selected from the D signal region. The X axis is the low $K_S^0\pi^0$ mass and the Y axis is the high $K_S^0\pi^0$ mass combination. The size of the symbol (X) is proportional to the number of entries in that bin.

where R is the ratio of the number of signal to background events in the D signal region; the fractions g_i are fixed to the values determined in the fit to the sideband region. The fit results are presented in Table III, and are shown in Fig. 8.

In order to check the level of interference, the fit was also performed with the assumption that there was no interference between the various amplitudes. The results are shown in Table III. We see that the fit fractions with and without interference are consistent with each other, suggesting that there is little interference. We also searched for $\bar{K}_0^*(1430)$ by including another Breit-Wigner function in the fit, obtaining a 90% C.L. upper limit of 12% relative to the yield for $\bar{K}^{*0}(892)$.

In Table IV we present information on the number of signal events and detection efficiencies. The systematic error includes the effect of varying the ratio of signal to background events in the D signal region, amount of $\bar{K}^{*0}$ in the background, various momentum cuts on the π^0's, ignoring the effect of the detector resolution on the $\bar{K}^{*0}$ width, etc. In addition, we removed the requirement that the D^0 come from a D^{*+}. In all cases, we obtain results which agree with those in Table III. In Table V we present a comparison between the present result, previous results, and theoretical predictions.

TABLE III. Results of Dalitz plot analysis.

Fit fraction of amplitudes	Dalitz plot fit with interference	Dalitz plot fit without interference
$\bar{K}^{*0}(892)$	$59.0^{+14.0}_{-11.0}\%$	$60.0^{+16.0}_{-12.0}\%$
$(\bar{K}^0\pi^0\pi^0)_{\mathrm{NR}}$	$37.0 \pm 8.0\%$	$40.0 \pm 10.5\%$
$\bar{K}^{*0}(892)$ phase	$67.0 \pm 14.0°$	

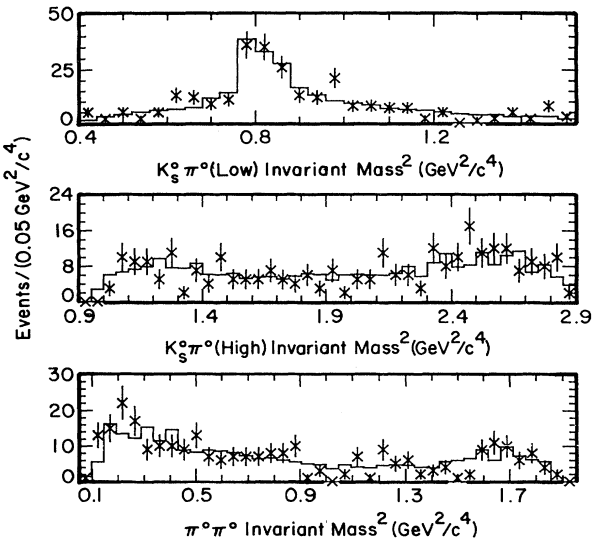

FIG. 8. Results of the Dalitz plot fit. The solid histogram is the fit, and the points are the projections of the Dalitz plot for events in the D signal region along the (a) $K^0_S\pi^0$ (low) mass^2, (b) $K^0_S\pi^0$ (high) mass^2, and (c) $\pi\pi$ mass^2 axes.

Using the results from the first column of Table III, the efficiencies from Table IV, and normalizing [29] to $D^0\to\bar{K}^0\pi^0$, we obtain

$$\frac{\mathcal{B}(D^0\to\bar{K}^{*0}\pi^0)}{\mathcal{B}(D^0\to\bar{K}^0\pi^0)}=1.65^{+0.39}_{-0.31}\pm0.20\ ,$$

$$\frac{\mathcal{B}(D^0\to(\bar{K}^0\pi^0\pi^0)_{\rm NR})}{\mathcal{B}(D^0\to\bar{K}^0\pi^0)}=0.37\pm0.08\pm0.04\ .$$

This implies $\mathcal{B}(D^0\to\bar{K}^{*0}\pi^0)=4.6^{+1.1}_{-0.9}\pm1.1\%$, and $\mathcal{B}(D^0\to(\bar{K}^0\pi^0\pi^0)_{\rm NR})=1.0\pm0.2\pm0.2\%$. The systematic error also includes the error in the branching ratio of the normalizing mode. See the Appendix for a numerical breakdown of the systematic error.

B. $D^0\to\bar{K}^{*0}\eta$

For this mode, $\bar{K}^{*0}$'s are detected in the $K^-\pi^+$ final state, and η via the $\gamma\gamma$ mode. To reduce background, we combine the $\bar{K}^{*0}\eta$ combination with a π^+ to form a D^{*+}, and impose a cut on the $D^{*+}-D^0$ mass difference. We require $X_{D^{*+}}\geq0.5$, and the $D^{*+}-D^0$ mass difference to be within 2.5 MeV/c^2 ($\sigma\approx0.85$ MeV/c^2) of the nominal mass difference. Since the $\bar{K}^{*0}$ has spin 1 and both D^0 and η have spin 0, this implies that the $\bar{K}^{*0}$ is emitted in the zero helicity state, with a $\cos^2\theta$ distribution, where θ is the angle between the K^- and the D^0 as seen in the $\bar{K}^{*0}$ rest frame. We thus require $|\cos\theta|>0.4$. In addition, the momentum of the η candidate is required to be greater than 0.5 GeV/c.

In Fig. 9 we present the invariant mass for the $K^-\pi^+\eta$ combinations, and in Fig. 10 the invariant mass for $K^-\pi^+$ combinations which fall within the (a) D signal region and (b) D sideband regions. The D signal, lower and upper sideband regions are defined to be 1.835–1.895, 1.78–1.81, and 1.91–1.94 GeV/c^2, respectively. Fitting the $K^-\pi^+$ invariant mass with a P-wave Breit Wigner for the D signal and sideband regions separately, we obtain 226±28 and 12±14 events, respectively. This leads to a net signal of 214±31 events. The efficiency, as shown in Table IV, includes the branching ratio of $\bar{K}^{*0}$ and η to observables.

We normalize this mode to $D^0\to K^-\pi^+\pi^0$ (measured branching fraction [16] =13.1±1.8%), and obtain

$$\frac{\mathcal{B}(D^0\to\bar{K}^{*0}\eta)}{\mathcal{B}(D^0\to K^-\pi^+\pi^0)}=0.13\pm0.02\pm0.03\ ,$$

implying $\mathcal{B}(D^0\to\bar{K}^{*0}\eta)=1.7\pm0.3\pm0.4\%$. We investigated various momentum cuts for the D^{*+} and η, helicity angle of the $\bar{K}^{*0}$, and also reconstructed the η via the

TABLE IV. Signal and efficiency for final states with $\bar{K}^{*0}$.

D decay mode	Decay of daughters	Number of events in signal	$\epsilon\mathcal{B}$[a]
$\bar{K}^{*0}\pi^0$	with a D^{*+} tag		
	$\bar{K}^{*0}\to K^0_S\pi^0$	122^{+29}_{-23}	0.90±0.05%
$(\bar{K}^0\pi^0\pi^0)_{\rm NR}$	with a D^{*+} tag	76±16	2.5±0.03%
$\bar{K}^{*0}\eta$	with a D^{*+} tag		
	$\eta\to\gamma\gamma$		
	$\bar{K}^{*0}\to K^-\pi^+$	214±31	3.8±0.17%
$K^-\pi^+\eta'$	with a D^{*+} tag		
	$\eta'\to\rho\gamma$	217±53	5.6±0.2%
	$\eta'\to\eta\pi^-\pi^+,\eta\to\gamma\gamma$	52±11	2.3±0.08%
	$\eta'\to\eta\pi^-\pi^+,\eta\to\pi^+\pi^-\pi^0$	17±5	0.8±0.04%
$K^-\pi^+\pi^0$	with a D^{*+} tag	10851±221	24.6±0.9%
$K^-\pi^+\pi^+\pi^-$	with a D^{*+} tag	8101±130	31.0±1.0%

[a]$\epsilon\mathcal{B}$ is the product of the efficiency to reconstruct this mode and the branching ratio of the D^0 daughter to observable particles.

TABLE V. Comparison of results for final states with $\bar{K}^{*0}$.

Results	$\bar{K}^{*0}\pi^0$	$\bar{K}^{*0}\eta$	$\bar{K}^{*0}\eta'$
This result	$4.6^{+1.1}_{-0.9}\pm1.1\%$	$1.7\pm0.3\pm0.4\%$	$<0.13\%$(90% C.L.)
Previous results			
Mark III [25]	$2.6\pm0.3\pm0.7\%$		
CLEO [21]		$2.3\pm0.7\pm1.0\%$	
E691 [31]		$<1.4\%$(90% C.L.)	
ARGUS [20]		$<2.6\%$(90% C.L.)	
Theory			
WSB without FSI's [1]	1.4%	0.3%	0.003%
WSB with FSI's [1]	3.9%	2.5%	
$1/N$, $N=\infty$ [5,24]	2.7%		
$1/N$, $N=3$	0.25%		
QCD sum rules [2]	3.1%	0.25%	
Donoghue [8]		$\geq 2.0\%$	

$\pi^+\pi^-\pi^0$ mode. In all cases, results were consistent with the above value. The systematic error contains contributions from the Monte Carlo efficiency, branching ratio of the normalizing mode, and the effect of various selection criteria. If the mean of the $\bar{K}^{*0}$ mass plot is allowed float in the fit, we get a slightly better fit, however, the yield changes by less than 10 events. We include this in the systematic error. See the Appendix for a numerical breakdown of the systematic error. In Table V, a comparison is presented between this result and others.

We also investigated the contributions due to final states like $K_1(1270)\eta$ and $Ka_0(980)$ by looking at the one-dimensional projections on the $K\pi$ and $\eta\pi$ mass axis. No signal was observed. The contribution of the $(K\pi\eta)_{\rm NR}$ final state is consistent with 0; the 90% C.L. upper limit is estimated to be 30% of the $\bar{K}^{*0}\eta$ final state.

C. $D^0\to\bar{K}^{*0}\eta'$

η''s are reconstructed in the $\rho\gamma$ and $\eta\pi^+\pi^-$ ($\eta\to\gamma\gamma$ and $\eta\to\pi^+\pi^-\pi^0$) final states. In Fig. 11, we present $K^-\pi^+\eta'$ invariant mass combinations for the three submodes. To reduce combinatoric background, the D^0 candidate is combined with a π^+ to form a D^{*+}. We require $X_{D^{*+}}>0.5$ and $M_{D^{*+}}-M_{D^0}$ to be within ±3.0 MeV/c^2 ($\sigma\approx1.0$ MeV/c^2) of the nominal mass difference. In Table IV, we present detailed information on this decay mode. Combining results from the three submodes [30] and normalizing to $D^0\to K^-\pi^+\pi^+\pi^-$ (branching ratio [16] $=9.1\pm1.1\%$) we obtain

$$\frac{\mathcal{B}(D^0\to K^-\pi^+\eta')}{\mathcal{B}(D^0\to K^-\pi^+\pi^+\pi^-)}=0.093\pm0.014\pm0.019\ .$$

This corresponds to $\mathcal{B}(D^0\to K^-\pi^+\eta')=0.85\pm$

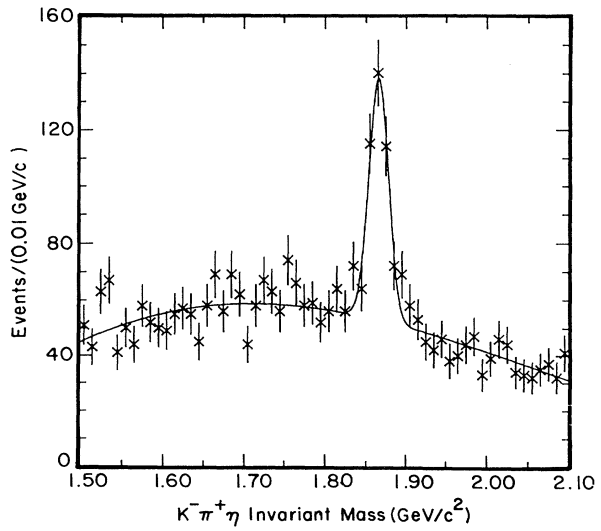

FIG. 9. Invariant mass $K^-\pi^+\eta$ ($\eta\to\gamma\gamma$) combinations for $X_{D^{*+}}>0.5$.

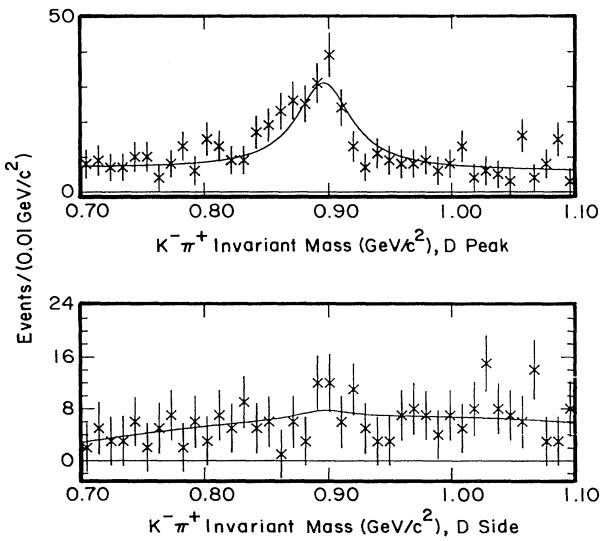

FIG. 10. $K^-\pi^+$ invariant mass for combinations which fall within (a) D signal region, (b) D sideband regions.

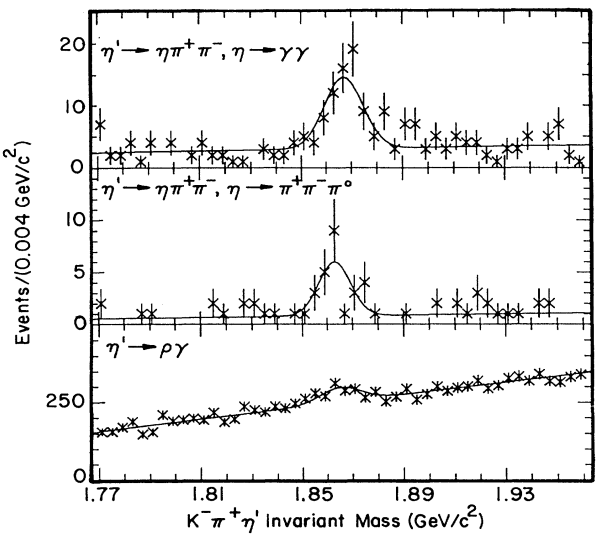

FIG. 11. Invariant mass of $K^-\pi^+\eta'$ mass combinations, with $X_{D^*} > 0.5$, for the three submodes.

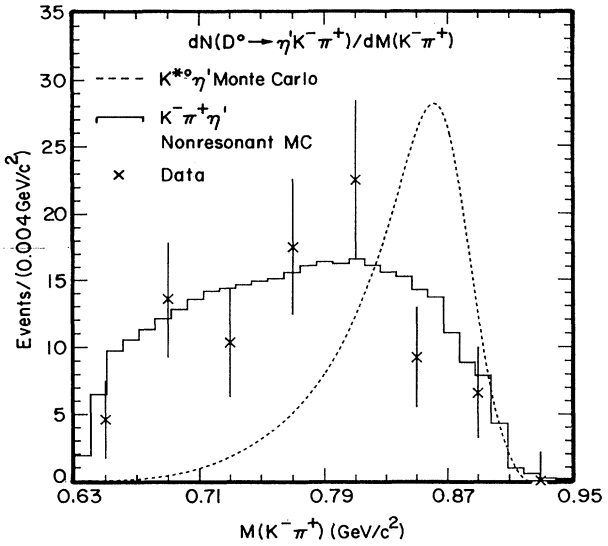

FIG. 12. D^0 yield in various $K^-\pi^+$ mass bins. The overlaid histograms are Monte Carlo simulations of nonresonant $K^-\pi^+\eta'$ production (dotted line), and resonant $\bar{K}^{*0}\eta'$ production, where $\bar{K}^{*0} \to K^-\pi^+$ (dashed line).

$0.13 \pm 0.20\%$. This represents the first measurement of this decay mode. The systematic error here too is estimated based on the spread in the results from the three submodes (in a manner similar to $D^0 \to \bar{K}^0\eta'$). It also includes the error in the branching ratio of the normalizing mode.

In order to extract the resonant contribution, we determine the D^0 yield in various $K^-\pi^+$ mass bins, as shown in Fig. 12; we use only the clean modes, i.e., $\eta' \to \eta\pi^+\pi^-$, where $\eta \to \gamma\gamma$ and $\eta \to \pi^+\pi^-\pi^0$. The points represent data; overlaid histograms are Monte Carlo simulations of nonresonant $K^-\pi^+\eta'$ production (dotted line), and resonant $\bar{K}^{*0}\eta'$ production, where $\bar{K}^{*0} \to K^-\pi^+$ (dashed line). The Monte Carlo distributions are arbitrarily normalized. In fitting the data with a combination of these two histograms, we have assumed that there is no interference between the two final states. The fit yields

$$\frac{\mathcal{B}(D^0 \to \bar{K}^{*0}\eta')}{\mathcal{B}(D^0 \to K^-\pi^+\eta')} < 0.15 (90\%\ \text{C.L.}) .$$

This implies $\mathcal{B}(D^0 \to \bar{K}^{*0}\eta') < 0.13\%$ (90% C.L.). This is the first information on $\mathcal{B}(D^0 \to \bar{K}^{*0}\eta')$. The branching ratio for this decay mode is expected to be heavily suppressed due to lack of phase space. The helicity angle distribution of the K^- (in the $K^-\pi^+$ rest frame) also favors nonresonant $K^-\pi^+\eta'$ production. In Table V, we compare this result with theoretical predictions.

V. SUMMARY AND CONCLUSIONS

The observed branching [7] ratio for $D^0 \to \bar{K}^0\phi (\approx 1\%)$ has been explained by Donoghue [8] to be due to scattering of the intermediate state $\bar{K}^{*0}\eta$, with the prediction that $\mathcal{B}(D^0 \to \bar{K}^{*0}\eta) \geq 2\%$. This is consistent with our measurement of $1.7 \pm 0.3 \pm 0.4\%$, as shown in Table V. Our measurement is also in agreement with previous results. The factorization models [1,4] have taken the observed value of $\mathcal{B}(D^0 \to \bar{K}^0\phi)$ as a quantitative measure of final-state interactions (FSI's), using it as an input to predict branching ratios for other $D^0 \to VP$ type decays.

We have also measured $\mathcal{B}(D^0 \to \bar{K}^{*0}\pi^0)$ via a Dalitz plot analysis of the reaction $D^0 \to K_S^0\pi^0\pi^0$, and our result is $4.6^{+1.1}_{-0.9} \pm 1.1\%$. This result is consistent with the Mark III result [25]. We do not find any evidence for $\bar{K}_0^*(1430)$, and set a 90% C.L. upper limit of 12% for the ratio $\mathcal{B}(D^0 \to \bar{K}_0^*(1430)\pi^0)/\mathcal{B}(D^0 \to \bar{K}^{*0}(892)\pi^0)$.

TABLE VI. Systematic errors for final states with $\bar{K}^0$.

Ratio of branching ratios	Cuts	MC simulation	Total
$(D^0 \to \bar{K}^0\pi^0)/(D^0 \to \bar{K}^0\pi^+\pi^-)$	7.0%	9.1%	11.4%
$(D^0 \to \bar{K}^0\eta)/(D^0 \to \bar{K}^0\pi^0)$ $\eta \to \gamma\gamma$	6.9%	6.4%	9.4%
$(D^0 \to \bar{K}^0\eta)/(D^0 \to \bar{K}^0\pi^+\pi^-)$ $\eta \to \pi^+\pi^-\pi^0$	6.6%	11.0%	12.9%
$(D^0 \to \bar{K}^0\eta')/(D^0 \to \bar{K}^0\pi^+\pi^-)$	See text for discussion		12.9%

TABLE VII. Systematic errors for final states with $\bar{K}^{*0}$.

Ratio of branching ratios	Cuts	MC simulation	Total
$(D^0\to\bar{K}^{*0}\pi^0)/(D^0\to\bar{K}^0\pi^0)$	8.2%	8.9%	12.1%
$(D^0\to\bar{K}^0\pi^0\pi^0)/(D^0\to\bar{K}^0\pi^0)$	8.2%	7.5%	11.1%
$(D^0\to\bar{K}^{*0}\eta)/(D^0\to K^-\pi^+\pi^0)$			
$\eta\to\gamma\gamma$	17.5%	8.7%	19.5%
$(D^0\to K^-\pi^+\eta')/(D^0\to K^-\pi^+\pi^+\pi^-)$	See text for discussion		20.4%

We have also made the first measurement of $\mathcal{B}(D^0\to(\bar{K}^0\pi^0\pi^0)_{\rm NR})=1.0\pm0.2\pm0.2\%$.

For $D^0\to\bar{K}^0\pi^0$, we measure the branching ratio to be $2.8\pm0.1\pm0.6\%$, which agrees with most previous measurements (with smaller errors), but disagrees with the latest result [22] from E691. We have also presented definitive measurements for $D^0\to\bar{K}^0\eta$, $D^0\to\bar{K}^0\eta'$, and $D^0\to K^-\pi^+\eta'$, and the first information on $D^0\to\bar{K}^{*0}\eta'$, as shown in Tables II and V.

Lipkin [10] has pointed out that D^0 decays to $\bar{K}^0\eta$ and $\bar{K}^0\eta'$ can be used to infer the presence of W-exchange diagrams. According to his arguments, excluding phase-space effects and neglecting FSI's, both these decay modes have approximately the same partial width for the internal W spectator diagram; however, for W-exchange diagrams $\bar{K}^0\eta'$ has a width roughly 10 times larger than $\bar{K}^0\eta$. This occurs because there are two competing diagrams resulting in these final states. In one diagram a $d\bar{d}$ is popped from the vacuum, and in the other a $s\bar{s}$ is popped from the vacuum [see Fig. 1(c)]. The η and η' have opposite phases for the $s\bar{s}$ quark content (η' is $u\bar{u}+d\bar{d}+s\bar{s}$, whereas η is $u\bar{u}+d\bar{d}-s\bar{s}$), thus there is constructive interference for $\bar{K}^0\eta'$ and destructive interference for $\bar{K}^0\eta$. The strength of the W-exchange diagrams relative to the internal W spectator diagram determines the final ratio of $\mathcal{B}(D^0\to\bar{K}^0\eta')/\mathcal{B}(D^0\to\bar{K}^0\eta)$. We measure this ratio to be 2.3 ± 0.4. Correcting for phase space, we measure the ratio of partial widths, $\Gamma(D^0\to\bar{K}^0\eta')/\Gamma(D^0\to\bar{K}^0\eta)=3.1\pm0.6$, which suggests the presence of W-exchange diagrams. In principle, one could also use $\bar{K}^{*0}\eta/\eta'$ final states, however, lack of phase space makes the latter state heavily suppressed.

The results of this analysis indicate that predictions of the factorization approach [1,4] agree better with data when FSI's are taken into account. The predictions of QCD sum rules [2] do not follow any systematic pattern, but on the whole seem to be lower than the observed values. The authors [2] claim that these predictions are valid to within a factor of 2, especially for decay modes where significant contributions from FSI's are expected. The $1/N$ approach [5] makes predictions which are consistent with our result, only in the limit $N=\infty$; however, there is some uncertainty in these predictions [24]. In summary, models of charm decay have made considerable progress in explaining nonleptonic decays of charm mesons; however, there is still a lot of scope for further study, especially in understanding the effect of final-state interactions and W-exchange mechanisms.

ACKNOWLEDGMENTS

We gratefully acknowledge the effort of the CESR staff in providing us with excellent luminosity and running conditions. J.P.A. and P.S.D. thank the PYI program of the NSF, I.P.J.S. thanks the YI program of the NSF, K.H. thanks the Alexander von Humboldt Stiftung, G.E. thanks the Heisenberg Foundation, K.K.G. and A.J.W. thank the TNRLC, K.K.G., H.N.N., J.D.R., and H.Y. thank the OJI program of DOE and R.P. and P.R. thank the A. P. Sloan Foundation for support. This work was supported by the National Science Foundation and the U.S. Department of Energy.

APPENDIX

In Tables VI and VII, we present a numerical breakdown of the various sources of systematic error in the *ratio of branching ratios;* they are listed as (a) cuts, which includes the effect of varying cuts, e.g., different momentum cuts on the D^0, helicity angle cuts, etc., and (b) Monte Carlo simulation, which includes the uncertainties in reconstructing tracks, photons, vee's, etc.; it also includes the errors due to *finite Monte Carlo statistics.* To reduce systematic errors, we have taken (wherever possible) ratios of D^0 decay modes which have the same number of tracks and photons in the final state. For this reason, we have shown the $D^0\to\bar{K}^0\eta$ submodes separately, since we normalize them to different modes ($D^0\to\bar{K}^0\pi^0$ and $D^0\to\bar{K}^0\pi^+\pi^-$).

The error(s) in the branching ratio of the normalizing mode(s) are not listed here. We have normalized our results to the Mark III results [16], which have errors of 17.2% for $D^0\to\bar{K}^0\pi^+\pi^-$, 13.7% for $D^0\to K^-\pi^+\pi^0$, and 12.1% for $D^0\to K^-\pi^+\pi^+\pi^-$. Comparing these errors with those presented in Tables VI and VII, one can see that in almost all cases, the experimental systematic error is smaller.

[1] M. Bauer, B. Stech, and M. Wirbel, Z. Phys. C **34**, 103 (1987).
[2] B. Yu. Blok and M. A. Shifman, Yad. Fiz. **45**, 841 (1987) [Sov. J. Nucl. Phys. **45**, 522 (1987)].
[3] L. L. Chau and H. Y. Cheng, Phys. Rev. D **36**, 137 (1987).
[4] F. Buccella, M. Lusignoli, G. Miele, and A. Pugliese, Z. Phys. C **55**, 243 (1992).
[5] A. J. Buras *et al.*, Nucl. Phys. **B268**, 16 (1986).

[6] A. N. Kamal and R. C. Verma, Phys. Rev. D **35**, 3515 (1987).
[7] Particle Data Group, K. Hikasa *et al.*, Phys. Rev. D **45**, S1 (1992).
[8] J. F. Donoghue, Phys. Rev. D **33**, 1516 (1986).
[9] I. I. Bigi, in *Heavy Quark Physics*, Proceedings of a Conference, Ithaca, New York, 1989, edited by P. S. Drell and D. L. Rubin, AIP Conf. Proc. No. 196 (AIP, New York, 1989).
[10] H. J. Lipkin, Phys. Rev. Lett. **46**, 1307 (1981).
[11] H. J. Lipkin, Phys. Lett. B **283**, 421 (1992).
[12] CLEO Collaboration, Y. Kubota *et al.*, Nucl. Instrum. Methods A **320**, 66 (1992).
[13] We require at least three charged tracks, visible energy greater than 0.15 of $E_{\text{c.m.}}$ and the primary vertex to be within 5 cm (in Z) of the interaction point.
[14] The asymmetric cut around the nominal ρ mass of 770 MeV/c^2 is applied because of the electric dipole nature of the $\eta' \to \rho\gamma$ transition. For instance, see G. Koop, T. Walsh, and P. Zerwas, Nucl. Phys. **B70**, 461 (1970).
[15] Detector simulation of all the decay modes presented here is performed using the GEANT package: GEANT 3.14 [R. Brun *et al.*, Report No. CERN DD/EE/84-1 (unpublished)].
[16] Mark III Collaboration, J. Adler *et al.*, Phys. Rev. Lett. **60**, 89 (1988).
[17] The individual branching ratios for the $\eta \to \gamma\gamma$ and $\eta \to \pi^+\pi^-\pi^0$ submodes are $0.89\pm0.11\pm0.20\%$ and $0.87\pm0.13\pm0.19\%$, respectively. The systematic errors on these branching ratios contain the error on the branching ratio of the normalizing modes. Since this error is common to both submodes, it is not averaged between them. Other systematic errors are added in quadrature to obtain the final systematic error.
[18] As a check, we have measured, in our data, the ratio of $\mathcal{B}(\eta \to \gamma\gamma)/\mathcal{B}(\eta \to \pi^+\pi^-\pi^0)$ to be 1.70 ± 0.10, which agrees well with the Particle Data Group [7] value of 1.64 ± 0.06. This comparison uses the Monte Carlo simulation to determine the reconstruction efficiencies for the two modes. We have included this discrepancy in the assessment of our systematic errors due to uncertainties in Monte Carlo simulation. See the Tables VI and VII.
[19] The ratio of branching ratios for the three submodes are $0.353\pm0.042\pm0.012(\eta' \to \rho\gamma)$, $0.306\pm0.027\pm0.011(\eta' \to \eta\pi^+\pi^-, \eta \to \gamma\gamma)$, and $0.27\pm0.045\pm0.013(\eta' \to \eta\pi^+\pi^-, \eta \to \pi^+\pi^-\pi^0)$. The second error quoted is the statistical error in our Monte Carlo sample. The confidence level of these three branching ratios coming from a common mean corresponds to 42.3%.
[20] ARGUS Collaboration, H. Albrecht *et al.*, Z. Phys. C **43**, 181 (1989).
[21] CLEO Collaboration, K. Kinoshita *et al.*, Phys. Rev. D **43**, 2836 (1991).
[22] E691 Collaboration, J. C. Anjos *et al.*, Phys. Rev. D **46**, R1 (1992). For purposes of comparison, the value quoted in Table II is obtained by using the measured ratio $\mathcal{B}(D^0 \to \bar{K}^0\pi^0)/\mathcal{B}(D^0 \to K^-\pi^+) = 1.36\pm0.23\pm0.22$, and the Mark III [16] value for $\mathcal{B}(D^0 \to K^-\pi^+) = 4.2\pm0.6\%$.
[23] ARGUS Collaboration, H. Albrecht *et al.*, Z. Phys. C **56**, 7 (1992).
[24] The predictions made in Ref. [5] depend on the ratio (η) of the QCD short-distance coefficients ($c_\pm$) in the effective Hamiltonian for $\Delta c = 1$ transitions. The authors have used $\eta = 2.4$, 2.8, and 3.2. We choose $\eta = 2.8$ for comparison. Choosing the lower (higher) value of η lowers (raises) the prediction for the decay rate (in units of s^{-1}) of internal spectator diagrams by about 32–38 %.
[25] Mark III Collaboration, J. Adler *et al.*, Phys. Lett. B **196**, 107 (1987).
[26] The J^P quantum numbers of $\bar{K}^{*0}(892)$ and $\bar{K}_0^*(1430)$ are 1^- and 0^+, respectively.
[27] M. Diakonou and F. Diakonos, Phys. Lett. B **216**, 436 (1989).
[28] The fractions g_i sum to 1. If there is no interference between the amplitudes in $\mathcal{L}_s$, then f_i's will necessarily add up to 1; however, in the presence of interference, f_i's need not add to 1.
[29] Using a D^{*+} tag for $D^0 \to \bar{K}^0\pi^0$, we detect 481 ± 24 events with an efficiency of $5.86\pm0.13\%$. We use these numbers in the normalization.
[30] The ratio of branching ratios for the three submodes, normalized to $D^0 \to K^-\pi^+\pi^+\pi^-$, are $0.149\pm0.036\pm0.005$ ($\eta' \to \rho\gamma$), $0.086\pm0.018\pm0.003$ ($\eta' \to \eta\pi^+\pi^-, \eta \to \gamma\gamma$), and $0.089\pm0.023\pm0.004$ ($\eta' \to \eta\pi^+\pi^-, \eta \to \pi^+\pi^-\pi^0$). The second error quoted in the error from limited Monte Carlo statistics, where the means and widths are floated in the data. Constraining the mean of, e.g., the value for $\eta' \to \eta\pi^+\pi^-, \eta \to \pi^+\pi^-\pi^0$ to match that observed for $\eta' \to \eta\pi^+\pi^-, \eta \to \gamma\gamma$ changes the total number of fitted D^0's in that decay chain by less than 5%. The confidence level of these three branching ratios coming from a common mean corresponds to 25%.
[31] E691 Collaboration, J. C. Anjos *et al.*, Phys. Rev. D **42**, 2414 (1990).